Int. J. Electrochem. Sci., 15 **(2020)** 11191 – 11202, doi: 10.20964/2020.11.24

International Journal of
ELECTROCHEMICAL
SCIENCE
www.electrochemsci.org

Effect of Nanosized Silicon Dioxide Additive on Plasma Electrolytic Oxidation Coatings Fabricated on Aluminium

Zhi-quan Huang[1], Rui-qiang Wang[2], Heng Zhang[3], Xiao-jie Shen[4], Xu-zhen Zhang[1], Yang He[5], Chen Huang[5], De-jiu Shen[1], Da-long Li[6,]*

[1] State Key Laboratory of Metastable Materials Science and Technology, College of Materials Science and Engineering, Yanshan University, Qinhuangdao 066004, China
[2] School of Material Science and Engineering, Beijing Institute of Technology, Beijing 100081, China
[3] Zhejiang Geely Automobile Co., Ltd. Ningbo 315800, China
[4] Chongqing Institute of Green and Intelligent Technology, Chinese Academy of Sciences
[5] Jiangsu Pacific Precision Forging Co., Ltd. Taizhou 225300, China
[6] College of Mechanical Engineering, Yanshan University, Qinhuangdao 066004, China
[*]E-mail: lidalong613@163.com

Received: 8 July 2020 / *Accepted:* 22 August 2020 / *Published:* 30 September 2020

Plasma electrolytic oxidation (PEO) of AA1060 aluminium was carried out in aluminate electrolytes to develop corrosion-resistant coatings. Different concentrations (0, 2 and 4 g/L) of a SiO_2 nanoparticle (n-SiO_2) additive and different treatment times of 15 min and 30 min were employed in this investigation. The PEO coatings were characterized by using a scanning electron microscopy (SEM) equipped with energy-dispersive X-ray spectroscopy (EDS), and X-ray diffraction (XRD). The corrosion resistances of each coating was evaluated by electrochemical methods. Results showed that n-SiO_2 hindered the formation of the α-Al_2O_3 phase and promoted the generation of the γ-Al_2O_3 and mullite phases. The addition fo n-SiO_2 in the electrolytes could shorten the breakdown time of PEO, enhance the breakdown voltage, reduce the number of pores in the electrolyte/coating (E/C) interface and enlarge the internal cavity. The coating formed after 15 min in a $NaAlO_2$ solution containing 4 g/L n-SiO_2 additive showed the best corrosion resistance, exhibiting the lowest corrosion current density of ~8.7×10^{-10} A/cm^2.

Keywords: Nanosilica; Plasma electrolytic oxidation； Pure aluminium

1. INTRODUCTION

Plasma electrolytic oxidation (PEO), also known as micro-arc oxidation (MAO), is a surface treatment technique developed from anodic oxidation to generate ceramic coatings on the valve metal surface [1]. During the process of plasma electrolytic oxidation, the electrolyte undergoes complex reactions such as electrochemical reaction, thermal reaction and plasma chemical reactions [2, 3]. Many

factors influence the PEO process, including the electrical parameters, composition and concentration of electrolyte, matrix materials, and temperature and pH parameters. These factors affect the thickness, porosity, structure and composition of the PEO coatings, thereby affecting their corrosion and wear resistance. Therefore, it is clear that the influencing factors during the PEO process play an important role in the formation of PEO coatings.

In recent years, nanocomposite coatings have been prepared by adding appropriate nanoparticles or powders into PEO electrolytes to improve the final properties of the coatings, such as their wear resistance, corrosion resistance and thermal conductivity [4, 5]. Depending on whether the nanoparticles react with the components of the coating after incorporation, the nanoparticles can be divided into reactive, partially reactive and inert [6]. Lu et al. believed that oxide particles can more easily achieve reactive incorporation into the coating in comparison to other kinds of particles [6]. The materials used as nanometer-scale oxide additives include MgO, TiO_2, ZrO_2, SiO_2, CeO_2 and Al_2O_3 [7-10]. The study of Toorani et al. [11] showed that PEO coating with α-Al_2O_3 particles had a better corrosion resistance than an m-ZrO_2 doped coating because the former has a larger thickness which plays a key role in improving the corrosion resistance of the coatings. Wu et al. [12] studied the various properties of PEO coatings formed on AZ31 Mg alloys in the electrolytes containing different concentrations of CeO_2 nanoparticles and concluded that adding CeO_2 nanoparticles with 3 g/L in the electrolyte was the optimal solution. Relatively speaking, however, the research on the addition of SiO_2 nanoparticles (n-SiO_2) has rarely been reported on pure aluminium. In this paper, the influences of n- SiO_2 and the PEO processing time on the structure and corrosion resistance of the coatings were studied. The application of long-term PEO treatments with each sample aimed to provide n-SiO_2 the opportunity to fully react with the coatings or substrate.

2. EXPERIMENTAL

2.1. Materials and the preparation of PEO coatings

Prior to the PEO process, the AA1060 aluminium with the size of 15 mm×15 mm×0.2 mm were grounded up to 3000 grit, then washed with distilled water, degreased ultrasonically in acetone and dried in room temperature air. The PEO treatment was carried out by a custom PEO process device that consisted of a high power supply unit (WH-1A), a stainless steel container, and an electrolyte cooling system to maintain the electrolyte temperature at 30±5 °C during the PEO process. Previous studies have reported that the addition of stabilizers composed of organic compounds may affect the electrochemical behaviour during the PEO process, thus affecting the growth and quality of the coatings [12, 13]. Therefore, to investigate the incorporation behaviour of nanoparticles, the stabilizer is replaced by a mechanical stirrer with the same effect [9]. The samples were treated under a pulsed AC electrical source with a duty ratio of 50% and a frequency of 50 Hz. The PEO electrolyte was prepared with deionized water containing 4 g/L $NaAlO_2$ and 1 g/L NaOH. Three various concentrations, 0, 2 and 4 g/L, of n-SiO_2 with a size of 30 nm were added to perform PEO coatings, and the corresponding electrical conductivities of the electrolytes were 7.26, 7.18 and 6.59 mS/cm, respectively.

The coatings were prepared at a constant current density of 4.4 A/dm^2 for 15 and 30 min. According to the concentrations of n-SiO_2 and the treatment times of the samples, the corresponding samples were named 0Si15, 0Si30, 2Si15, 2Si30, 4Si15, and 4Si30. The PEO process parameters are shown in Table 1. After the PEO treatment, the samples were washed with deionized water, immersed in deionized water for 12 h and then dried under normal atmospheric conditions.

Table 1. Composition of electrolytes and PEO treatment time used in this study.

Samples	Concentration of n-SiO_2, g/L	Treatment time, min
0Si15	0	15
0Si30	0	30
2Si15	15	15
2Si30	15	30
4Si15	20	15
4Si30	20	30

2.2. Testing equipment and process

During the PEO process, the cell voltages were recorded with a sampling time of 1 ms using a USB4702 data acquisition system controlled by Wave Scan software (USB-4702, Advantech Co., Ltd.). The morphologies of the electrolyte/coating (E/C) interface, coating/substrate (C/S) interface and fractured cross-section of the PEO coatings formed under different conditions were observed by using scanning electron microscopy (SEM, Hitachi S-4800). After the PEO process, some of the coatings were detached from the substrate utilizing the patented electrochemical method to investigate the coating morphologies at the C/S interface [14]. A study on the phase composition of coatings was performed by using an X-ray diffraction (XRD, D/MAX-rB) with a Cu Ka radiation source at 40 kV and 200 mA and a scanning rate of 2°/min over a 2θ range of 10° to 80°. Polarization tests were measured using a RST5000 Electrochemical Workstation, to evaluate the electrochemical corrosion behavior of the PEO coatings. After the electrochemical testing system became stable, potentio-dynamic polarization test scanning was conducted at a rate of 1 mV/s in 3.5 wt.% NaCl solution. An exposed area of 1 cm^2 of the test sample was kept in contact with the test solution. Before performing the electrochemical tests, all the samples were exposed to the test solution for 0.5 h to attain a stable open circuit potential. The corrosion cell consists of a saturated calomel electrode (SCE) as the reference electrode, a platinum foil as the counter electrode. The obtained EIS data was analysed by equivalent circuit modelling using ZSimpwin software.

3. RESULTS AND DISCUSSION

3.1. Voltage-time response during the PEO process

The voltage-time responses of the different concentrations of n-SiO_2 particles are shown in Fig.

1. The increasing rate of the voltage, the corresponding breakdown voltage and the corresponding terminal voltage increase during the PEO process as the concentrations of n-SiO_2 increases, respectively. This result may be caused by the influences of the n-SiO_2 particles on the formation and characteristics of the coatings.

At the initial stage of the PEO process, which is generally considered the traditional anodic oxidation stage, the voltage increases linearly with the processing time, and the dissolution of the substrate and the formation of the passive film at the E/C interface of the substrate are carried out simultaneously [15-17]. At this time, there is no discharge spark formation on the sample, only galvanoluminescence and emission phenomena. Once the critical breakdown voltage is reached, the weakest part of the passive film is broken down accompanied by the emergence of plasma discharges, and the reaction goes from the traditional anodic oxidation stage to the plasma electrolytic oxidation stage [18].

After the initial stage, an inflection appears in each voltage-time curve, so that the increasing rate of operating voltage starts to gradually decrease. It is generally considered that the inflection in the voltage curve is associated with the onset of the dielectric breakdown of the film [18, 20]. The breakdown voltages for samples 0Si30, 2Si30, and 4Si30 were observed to be 526.4, 548.4 and 576.4 V, respectively. There are two reasons for the increasing breakdown voltage. First, under the action of an electric field and mechanical stirring, particles with a negative ζ-potential can easily move to the E/C interface of the anode sample. Then, the E/C interface of the coatings adsorb silica particles, which increases the resistance value of the coatings and further increases the oxidation voltage. Second, a higher voltage is needed to overcome the resistance of the dielectric layer at low conductivity to induce a spark at the E/C interface of the substrate. Therefore, the sample 4Si30 has a higher breakdown voltage than the other samples. To reduce the influence of the edge effect on the whole experiment, the following tests were performed in the middle part of the coatings [21-23]. Furthermore, the PEO process carried out at a high concentration of n-SiO_2 (4 g/L, sample 4Si30) electrolyte transitions to the second stage earlier than the PEO process without n-SiO_2 (sample 0Si30), and the rate of increasing voltage is also much higher than that of 0Si30. This result in Fig. 1 indicates that the higher the concentration of n-SiO_2 is, the higher applied voltage required for dielectric breakdown and the faster development of the discharge.

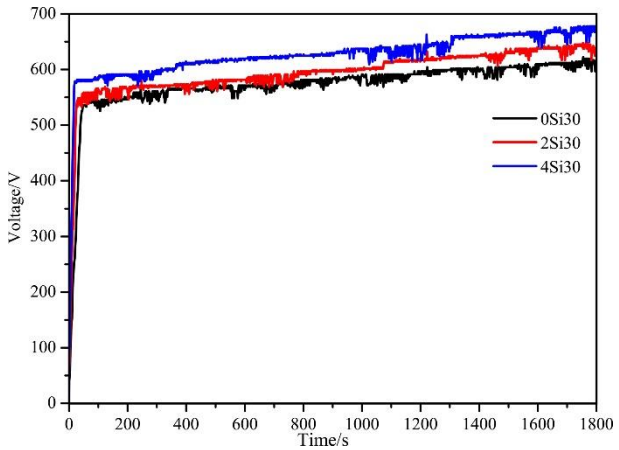

Figure 1. Corresponding voltage vs. time curves during the PEO process. (0Si30: with n-SiO_2 of 0 g/L for 30 min, 2Si30: with n-SiO_2 of 2 g/L for 30 min, and 4Si30: with n-SiO_2 of 4 g/L for 30 min).

3.2 Phase composition

The XRD patterns for the coatings of the above samples are presented in Fig. 2. Strong peaks of Al present in the XRD patterns of all samples are detected correspond to the substrate. Comparing the PDF (Powder Diffraction File) card identified that the phases of the ceramic layers are different, but they all contain a main phase α-Al_2O_3 phase and a small amount of the γ -Al_2O_3 phase. Two additional phases (SiO_2 and mullite), which are more evident with samples 4Si15 and 4Si30, are also clearly detected in addition to γ- and α-Al_2O_3. The study by Rachida found that the formation of mullite is mainly related to the calcination temperature and the type of starting material and that mullite cannot be generated by the reaction of α-Al_2O_3 with silica in either a crystalline or amorphous state [24]. During the formation of the mullite phase, n-SiO_2 can diffuse into the γ-Al_2O_3 crystal lattice, substitute Al atoms and change the phase transformation kinetics of the alumina phases, thereby inhibiting the phase transformation of γ-Al_2O_3 to α-Al_2O_3. Therefore, the peak intensity of α-Al_2O_3 weakens and the peak intensity of the γ-Al_2O_3, SiO_2 and mullite phases strengthen with increasing n-SiO_2 concentratio, as shown in Fig. 2.

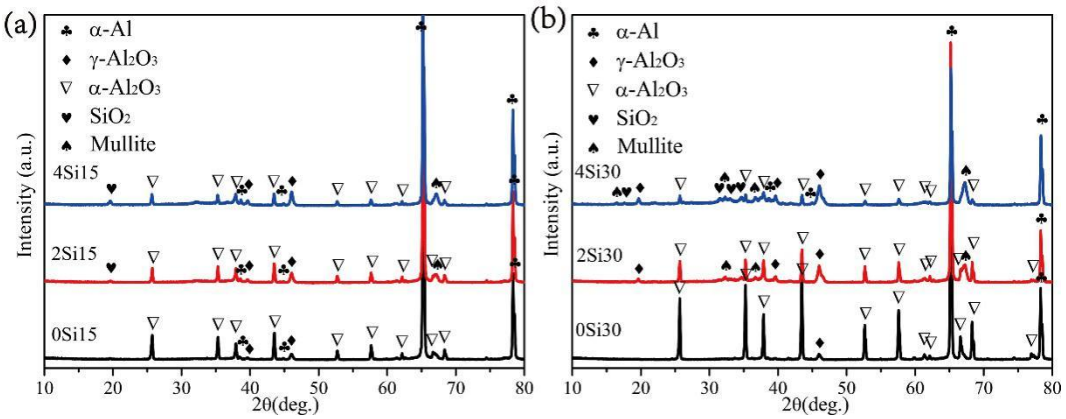

Figure 2. XRD spectra of the PEO coatings formed under different conditions in Table 1.

3.3 Morphological observations of the E/C interfaces

As shown in Fig. 3, the SEM images of the E/C interfaces of the samples produced in electrolytes with different contents of n-SiO_2 particles for 15 and 30 min of PEO treatments are presented. From Fig. 3a, we can see that the E/C interfacial morphology of the 0Si15 coating is mainly composed of pores and a nodular morphology, while the pores can be divided into long and narrow pores and small round pores. In addition to, pancake-like structures appear on the E/C interface of sample 2Si15 (Fig. 3c) and sample 4Si15 (Fig. 3e), with these structures being more obvious on the latter. Compared with Fig. 3a, 3c and 3e, it can be found that when the PEO treatment time is 15 min, the size of the pores, especially the narrow and long pores, tends to decrease with the increase in the concentration of n-SiO_2. With the increase in concentration of n-SiO_2 particles, a higher applied voltage is used to meet the higher breakdown voltage of the coatings, resulting in an environment with a stronger electric field. The stronger electric field aggravates the B-type discharge, thus generating a higher temperature. Since B-

type discharge can penetrate the whole coating [2], intensifying the B-type discharge will increase the amount of the molten substrates and produce more oxides in the subsequent process. Serried molten oxides that are produced as high temperature reatively weaken the cooling effect of the surrounding electrolyte, thus facilitating the flow-back and filling actions of the molten materials [25]. The flow-back and filling of molten oxide decrease the size of micropores at the E/C interface.

From Fig. 3 we can see that, regardless of the content of n-SiO_2, the E/C interfaces have high porosity when the PEO treatment time is 15 min, while the E/C interfaces are mainly pancake-like structures when the PEO treatment time is 30 min. Compared with the E/C interface of sample 2Si15(Fig. 3c) and 4Si15 (Fig. 3e), the pancake-like morphology coexists with the micropores, suggesting that the PEO process of the sample is more vigorously as the concentration of n-SiO_2 increases. What is more, with the increase of n-SiO_2 concentration, the initiation time of the plasma discharge is shortened, thus accelerating the transformation from micropores to pancake-likes structures. The essence of this accelerated transformation is the improvement in the molten flow-back and filling actions by the more intense plasma discharges.

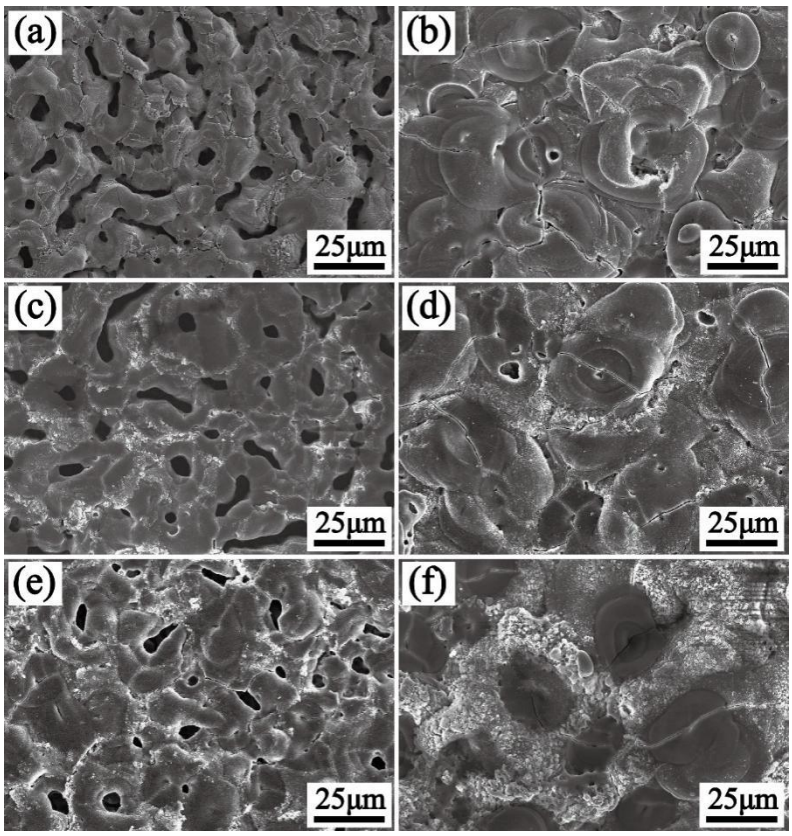

Figure 3. E/C interfacial morphologies of the PEO coatings:.(a) 0Si15, (b) 0Si30, (c) 2Si15, (d) 2Si30, (e) 4Si15, and (f) 4Si30.

3.4 Fractured cross-sectional morphology

As shown in Fig. 4, the detached coatings can clearly show the internal structure of the coatings.

It can be seen that there is a continuous, thin, scalloped, and compact layer with some small hemisphere and many cavities or channels on it. From the Fig. 4, it can be seen that at the same PEO processing time, the coating thickness and the size of the cavities increases with the increase in the content of n-SiO_2. In addition, it can be seen that the thickness and cavity volume of the coatings formed in 30 min are much bigger than those of the coatings formed in 15 min.

It is clear from Fig. 4 that the fractured C/S interface of the coatings has a good continuity. The barrier layer thickness of sample 0Si30 is slightly increased compared with that of sample 0Si15, while the thickness of the barrier layer of the coatings obtained in the n-SiO_2-containing electrolytes is not significantly different with the extending of PEO time. The barrier layer thickness of samples 2Si15 and 4Si15 are significantly higher than that of sample 0Si15. However, when the PEO treatment time arrives 30 min, there is no significant difference in the barrier layer thickness of samples 0Si30, 2Si30 and 4Si30.

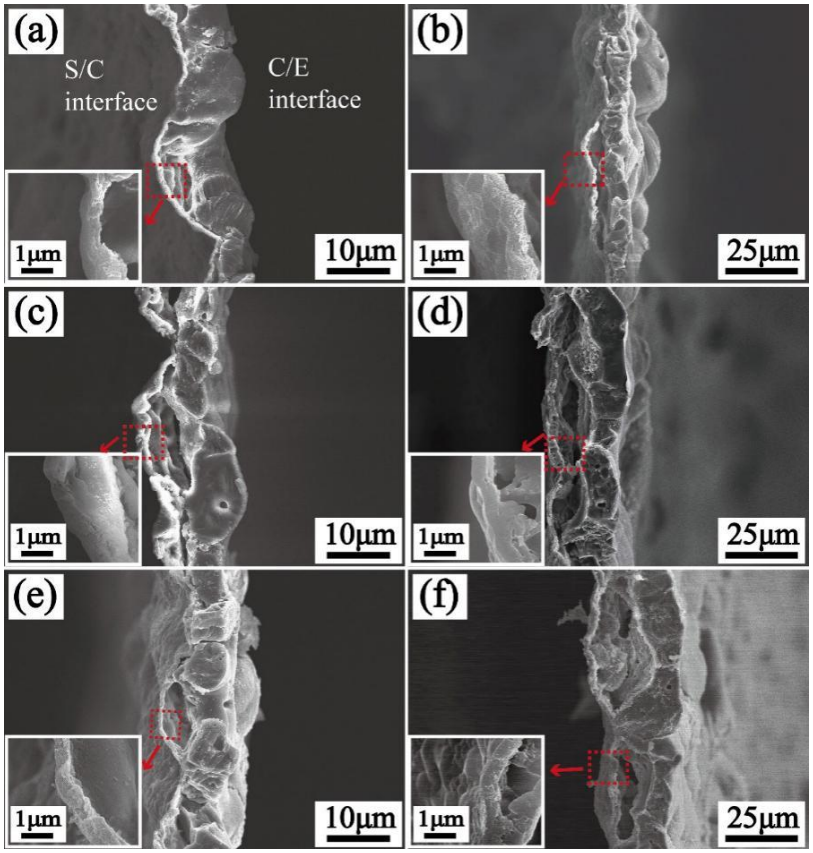

Figure 4. Cross-sectional microstructures of the PEO coatings: (a) 0Si15, (b) 0Si30, (c) 2Si15, (d) 2Si30, (e) 4Si15, and (f) 4Si30.

3.5 C/S interface morphology

The C/S interfacial morphologies of coatings are shown in Figs. 5, we can see that the C/S interfaces are composed of many irregular protrusions. These irregular protrusions correspond to cavities in the fractured cross-sectional morphology [25]. The irregular protrusions have sharp outlines and distinct boundaries with each other. With time, the size of irregular protrusions gradually increased and

the boundary slowly blurred when the PEO time reaches 30 minutes. In combination with the cross-sectional microstructures shown in Fig. 4 and the C/S interfacial microstructures in Fig. 5, it can be found that the barrier layer is formed by a combination of the hemispherical oxide. Under the same experimental conditions, there is no significant difference in the hemispherical diameter of the coatings, indicating that the diameter of the hemispherical structure is independent of the PEO time and the addition of nanoparticles. With the extension of the PEO time, the discharge at the C/S interface of the coatings gradually becomes intense and dense, thus consuming the substrate by producing more molten substrate and exposing fresh substrate. When the discharge extinguishes, the molten and newly exposed substrate are oxidized and quenched into a new oxide coating. The irregularly shaped protrusions are the oxide coatings which formed at the position of the consumed substrate. Therefore, the protrusion size (Fig. 4) and the fluctuation at the C/S interface (Fig. 5) become larger and larger with the long-term PEO treatment.

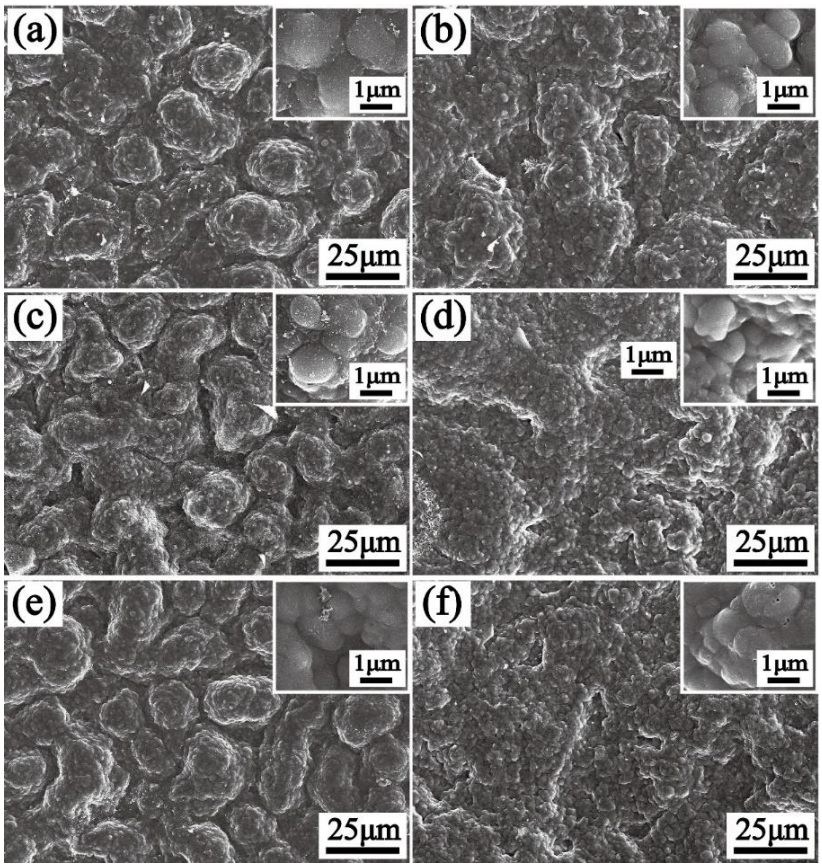

Figure 5. C/S interfacial microstructures of the PEO coatings: (a) 0Si15, (b) 0Si30, (c) 2Si15, (d) 2Si30, (e) 4Si15, and (f) 4Si30.

3.6 Corrosion behaviour

Fig. 6 shows potentiodynamic polarization curves in 3.5% NaCl solution, which is used to evaluate corrosion resistance of the PEO coatings. Corrosion potential (E_{corr}), corrosion current density (i_{corr}), and anodic/cathodic Tafel constants (b_a and b_c) are given in Table 2.. The corrosion potential (E_{corr})

reflects the probability of corrosion in the test solution. The higher the corrosion potential is, the lower possibility of being an anode, thus, the lower corrosion probability. The corrosion current (i_{corr}) reflects the corrosion rate of the actual corrosion reaction.

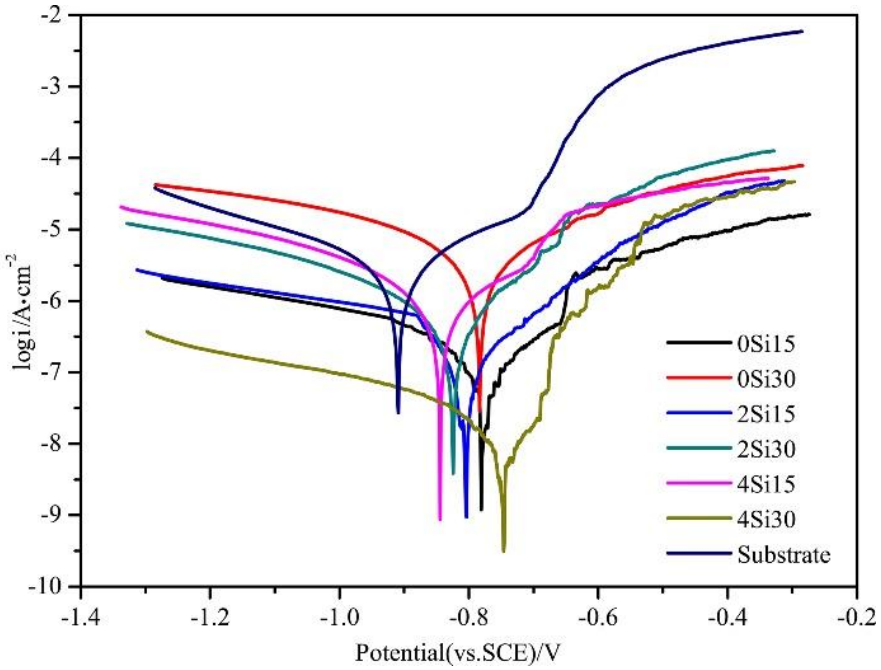

Figure 6. The potentiodynamic polarization curves of the substrate and PEO-coated samples at a rate of 1 mV/s in 3.5 wt.% NaCl solution.

Table 2. Electrochemical properties of the potentiodynamic polarization curves derived from Fig 6.

Samples	E_{corr}(mV/sec)	i_{corr}(Acm^{-2})	b_a(mV/decade)	b_c(mV/decade)	R_p(kΩcm^2)
Substrate	-907	1.7×10^{-7}	67	82	97.5
0Si15	-762	4.8×10^{-8}	47	121	309.9
0Si30	-784	1.2×10^{-7}	82	71	139.1
2Si15	-809	2.1×10^{-8}	75	55	666.8
2Si30	-821	3.7×10^{-8}	58	76	387.8
4Si15	-844	8.7×10^{-10}	75	73	18389.1
4Si30	-749	1.8×10^{-9}	87	76	9564.8

The lower the corrosion potential is, the lower the corrosion rate of the corrosion reaction will be. The polarization resistance reflects the reaction rate of the anode and cathode after the beginning of

corrosion. The higher the polarization resistance is, the stronger the relative corrosion resistance. The polarization resistance (R_p) is calculated using the Stern-Geary equation[26] :

$$R_P = \frac{b_a \times b_c}{2.303 i_{corr}(b_a + b_c)} \quad (2)$$

It can be clearly observed from Table 2 that the current densities and the polarization resistances of the PEO-treated coatings are lower and higher than that of the substrate, respectively, which indicates that the corrosion resistance of PEO-treated coatings is better than that of the substrate. At the same time, a more negative corrosion potential of the substrate gives a demonstration of a more obvious corrosion tendency than PEO coated samples. With the prolongation of PEO treatment time, the current density increases and the corrosion resistance decreases with or without additives, respectively. The reason for the increase of corrosion resistance is that the n-SiO_2 additive play an important role for the conformation of dense barrier layer. The enlargement of cavity makes it easier for corrosion fluids to pass through the outer layer and eventually reach the inner barrier layer, which causes the increasing of the actual exposed area of the inner barrier layer.

It can be seen from Table 2 that the coatings in the electrolyte with additive have smaller current density and higher polarization resistance compared with the coatings formed in the electrolyte without additive, that means the coatings with n-SiO_2 additive have better corrosion resistance than that without additive. As displayed in Table 2, the 4Si15 coating shows the excellentest corrosion resistance, since it has the lowest corrosion current density and the largest polarization resistance than the others. The outstanding corrosion resistance of 4Si15 coating indicates a good barrier effect on the transfer of Cl^- during potentiodynamic polarization. Under the same PEO time, the thickness of the dense inner barrier layer gradually increases with the increase of the additive concentration, indicating that the transport of Cl^- is more and more difficult and the corrosion resistance gradually increases. Although the cavity size of the 4Si15 coating is slightly larger than that of the 2Si15 and 0Si15 coatings, the 4Si15 coating has fewer holes and cracks than the 2Si15 and 0Si15 coatings in the E/C interfacial topography (Fig. 3). Therefore, the corrosion resistance is not only affected by the holes and cracks in the outer layer, but also by the thickness of the inner dense barrier layer.

4. CONCLUSIONS

In this study, the effects of electrolytes with different concentrations of n-SiO_2 on the corrosion resistance and structural characteristics of PEO samples in 15 and 30 min are analyzed by investigating the breakdown voltages, the E/C interface and C/S interface and cross-sectional morphologies, phases compositions, and potentiodynamic polarization curves. The experimental results show the following:

(1) With the addition of n-SiO_2 particles, the progress of PEO was promoted, showing that the breakdown time becomed shorter, and the breakdown voltage and termination voltage decreased.

(2) The results show that the additives directly affect the formation of phases. Except for α -Al_2O_3 and γ-Al_2O_3 constitute the common phases in the coatings, particularly phases, SiO_2 and mullite were detected in the coatings with n-SiO_2, respectively. In addition, the generation of α-Al_2O_3 was inhibited in the coatings with n-SiO_2.

(3) The additive of n-SiO_2 can reduce the number of pores and cracks at the E/C interface, which is beneficial for improving the coating thickness. With an extended PEO time, the E/C interface of the coating changes from a porous morphology to a pancake-like morphology, with a constant increase of irregularly shaped protrusions composed of hemispherical oxide particles at the C/S interface.

(4) The potentiodynamic polarization curves show that the PEO treatment with the addition of n-SiO_2 can improve the corrosion resistance of the samples, and the corrosion resistance gradually increased and decreased with the increase of the concentration and the extension of time, respectively.

ACKNOWLEDGMENTS
This work was supported by the National Natural Science Foundation of China (No. 51671167).

References

1. A.L. Yerokhin, X. Nie, A. Leyland, A. Matthews, and S.J. Dowey, *Surf. Coat. Technol.* 122 (1999) 73.
2. R.O. Hussein, X. Nie, D.O. Northwood, A. Yerokhin and A. Matthews, *J. Phys. D: Appl. Phys.*, 43 (2010) 105203.
3. R.O. Hussein, X. Nie and D.O. Northwood, *Electrochim. Acta*, 112 (2013) 111.
4. M. Kaseem, H.L. Yong and Y.G. Ko, *Mater. Lett.*, 182 (2016) 260.
5. X. Lu, C. Blawert, K.U. Kainer and M.L. Zheludkevich, *Electrochim. Acta*, 196 (2016) 680.
6. X. Lu, M. Mohedano, C. Blawert, E. Matykina, R. Arrabal and K.U. Kainer, *Surf. Coat. Technol.,* 307 (2016) 1165.
7. X.T. Liu, D.D. Wang, Y.K. Wu, Z. Yang, D. Li and D. Shen, *Int. J. Appl. Ceram. Technol.,* 17 (2020) 1017.
8. E. Matykina, R. Arrabal, P. Skeldon and G.E. Thompson, *J. Appl. Electrochem.,* 38 (2008) 1375.
9. S. Fatimah, M.P. Kamil, J.H. Kwon, M. Kaseem and Y.G. Ko, *J. Alloy. Compd.,* 707 (2016) 358.
10. T. Arunnellaiappan, S. Arun, S. Hariprasad, S. Gowtham, B. Ravisankar and L.R. Krishna, *Ceram. Int.,* 44 (2018) 874.
11. M. Toorani, M. Aliofkhazraei and A.S. Rouhaghdam, *Surf. Coat. Technol.,* 352 (2018) 561.
12. D. Wu, X. Liu, K. Lu, Y. Zhang and H. Wang, *Appl. Surf. Sci.,* 255 (2009) 7115.
13. A. Bai and Z.J. Chen, *Surf. Coat. Technol.,* 203 (2009) 1956.
14. C. Liu, D. He, Q. Yan, Z. Huang, P. Liu , D. Li , G. Jiang , H. Ma, D. Shen and P. Nash, *Surf. Coat. Technol.,* 280 (2015) 86.
15. Y. Cheng, F. Wu, E. Matykina, P. Skeleton and G.E. Thompson, *Corrosion Sci.,* 59 (2012) 307.
16. Y. Cheng, M.K. Mao, J.H. Cao and Z.M. Peng, *Electrochim. Acta*, 138 (2014) 417.
17. Y. Zhang, Y. Wu, D. Chen, R. Wang, D. Li, C. Guo, G. Jiang, D. Shen, S. Yu and P. Nash, *Surf. Coat. Technol.,* 321 (2017) 236.
18. J. M. Albella, I. Montero, J.M. Martínez-Duart and V. Parkhutik, *J. Mater. Sci.,* 26 (1991) 3422.
19. S. Ikonopisov, *Electrochim. Acta*, 22 (1977) 1077.
20. L.O. Snizhko, A.L. Yerokhin, N.L. Gurevina, V.A. Patalakha and A. Matthews, *Thin Solid Films,* 516 (2007) 460.
21. J. Martin, A. Melhem, I. Shchedrina, T. Duchanoy, A. Nominé, G. Henrion, T. Czerwiec and T. Belmonte, *Surf. Coat. Technol.,* 221 (2013) 70.
22. D.D. Wang, X.T. Liu, Y. Su, Y.K. Wu, Z. Yang, H.-P. Han, X.Z. Zhang, G.R. Wu and D.J. Shen, *Surf. Eng.,* 36 (2020) 184.
23. A. Melhem, G. Henrion, T. Czerwiec, J.L. Briançon, T. Duchanoy, F. Brochard and T. Belmonte, *Surf. Coat. Technol.,* 205 (2011) S133.

24. R. El Ouatib, S. Guillemet, B. Durand, A. Samdi, L. Er Rakho and R. Moussa, *J. Eur. Ceram. Soc.,* 25 (2005) 73.
25. Y. Wu, Z. Yang, R. Wang, G. Wu, D. Chen, D.D. Wang, X.T. Liu, D.L. Li, C. Guo, S. Yu, D. Shen and P. Nashd, *Surf. Coat. Technol.,* 351 (2018) 136.
26. Th. von Kármán, H.W. Emmons, T. Geoffrey, R.S. Tankin Von Kármán, *J. Electrochem. Soc.,* 104 (1957) 751.